

Manuscript version: Author's Accepted Manuscript

The version presented in WRAP is the author's accepted manuscript and may differ from the published version or Version of Record.

Persistent WRAP URL:

<http://wrap.warwick.ac.uk/103362>

How to cite:

Please refer to published version for the most recent bibliographic citation information. If a published version is known of, the repository item page linked to above, will contain details on accessing it.

Copyright and reuse:

The Warwick Research Archive Portal (WRAP) makes this work by researchers of the University of Warwick available open access under the following conditions.

Copyright © and all moral rights to the version of the paper presented here belong to the individual author(s) and/or other copyright owners. To the extent reasonable and practicable the material made available in WRAP has been checked for eligibility before being made available.

Copies of full items can be used for personal research or study, educational, or not-for-profit purposes without prior permission or charge. Provided that the authors, title and full bibliographic details are credited, a hyperlink and/or URL is given for the original metadata page and the content is not changed in any way.

Publisher's statement:

Please refer to the repository item page, publisher's statement section, for further information.

For more information, please contact the WRAP Team at: wrap@warwick.ac.uk.

Voltammetric Perspectives on the Acidity Scale and H^+/H_2 Process in Ionic Liquid Media

Cameron L. Bentley,¹ Alan M. Bond,² and Jie Zhang²

¹Department of Chemistry, University of Warwick, Coventry CV4 7AL, United Kingdom; email: C.Bentley.1@warwick.ac.uk

²School of Chemistry and Australian Research Council Centre of Excellence for Electromaterials Science, Monash University, Clayton, Victoria 3800, Australia; email: Alan.Bond@monash.edu, Jie.Zhang@monash.edu

Keywords

ionic liquids, acid/base chemistry, cyclic voltammetry, hydrogen evolution reaction, hydrogen oxidation reaction

Abstract

Nonhaloaluminate ionic liquids (ILs) have received considerable attention as alternatives to molecular solvents in diverse applications spanning the fields of physical, chemical, and biological science. One important and often overlooked aspect of the implementation of these designer solvents is how the properties of the IL formulation affect (electro)chemical reactivity. This aspect is emphasized herein, where recent (voltammetric) studies on the energetics of proton (H^+) transfer and electrode reaction mechanisms of the H^+/H_2 process in IL media are highlighted and discussed. The energetics of proton transfer, quantified using the $\text{p}K_{\text{a}}$ (minus logarithm of acidity equilibrium constant, K_{a}) formalism, is strongly governed by the constituent IL anion, and to a lesser extent, the IL cation. The H^+/H_2 process, a model inner-sphere reaction, also displays electrochemical characteristics that are strongly IL-dependent. Overall, these studies highlight the need to carry out systematic investigations to resolve IL structure and function relationships in order to realize the potential of these diverse and versatile solvents.

1. INTRODUCTION

Ionic liquids (ILs) possess physicochemical properties that are identical to those of molten salts. However, practical aspects regarding their use, maintenance, and handling are sufficiently different to warrant a distinction (1, 2). ILs are arbitrarily defined as any ionic compound with a melting point or glass transition below the boiling point of water at 1 atm pressure (i.e., 100°C) (3). The ILs discussed herein are of the so-called second/third generation air/water stable nonhaloaluminate class (2, 4, 5). Interest in ILs in both academia and industry for use in a range of applications has increased dramatically over the last 25 years (2, 6, 7). They are versatile solvents, and have been employed as replacements for volatile organic compounds in green synthesis (8, 9), separations (10), clean catalysis (11), and as electrolytes in electrochemical devices (1, 12, 13). In addition, ILs have found application in the biosciences, being employed as media for enzymatic reactions (14) and solubilization of biomolecules (15). In this review, a brief introduction to the general structure and physicochemical properties of ILs is presented, followed by an in-depth discussion on the energetics (thermodynamics) of proton transfer (i.e., equilibrium acidity) and electrochemical mechanisms of the H^+/H_2 process in this class of solvent.

1.1. Structure of Ionic Liquids

Although all ILs are often treated collectively as a class of solvent, the physicochemical properties (e.g., melting point, viscosity, polarity, solvating ability) of each formulation are uniquely determined by the nature of the constituent cation and anion. The chemical structures and general properties of the cations and anions that constitute commonly encountered aprotic and protic ILs are considered below.

1.1.1. Aprotic ionic liquids.

Aprotic ionic liquids (AILs) are those which contain no dissociable protons in their structures. The constituent cations of AILs tend to be organic, bulky, and asymmetric, with extensively shielded or delocalized charge (i.e., they are weak Lewis acids). Altering the chain length of the alkyl substituents on the cation influences the physicochemical properties of the resulting IL (e.g., melting point, hydrophobicity, and viscosity), which allows fine-tuning to a particular application (3, 16). The anions of AILs tend to be inorganic with highly diffuse or delocalized charge. They are typically weak Lewis bases and poor hydrogen bond acceptors. The

hydrophilicity/hydrophobicity, and thus, the level of water-miscibility of an IL, are largely determined by the choice of anion (3, 17, 18).

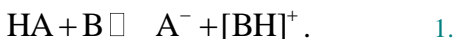
The diffuse, shielded, or delocalized charge on the constituent anion and/or cation of an IL results in intermolecular forces that are relatively weak compared to traditional ionic compounds. This translates to a relatively low lattice energy (further lowered by inefficient packing due to cation asymmetry), which is why these compounds are liquid at or below 100°C. It is important to note, however, that the cohesive forces operating within an IL are strong relative to those operating in most conventional molecular solvents, and for this reason, ILs often possess negligible vapor pressures and relatively high viscosities (1, 3). The names, abbreviations, and structures of a range of commonly encountered AIL cations and anions are summarized in Figure 1.

<COMP: PLEASE INSERT FIGURE 1 HERE>

Figure 1 Names, abbreviations, and structures of a range of commonly encountered IL cations and anions. Cations: 1-alkyl-3-methylimidazolium, [C_xmim]⁺; 1-alkyl-2,3-methylimidazolium, [C_xdmim]⁺; 1-alkyl-1-methylpyrrolidinium, [C_xmpyr]⁺; tetraalkylammonium, [N_{w,x,y,z}]⁺; trialkylsulfonium [S_{x,y,z}]⁺; mono/di/tri-alkyl-ammonium [N_{H,x,y,z}]⁺; alkyl-imidazolium [C_ximH]⁺; alkyl-pyrrolidinium [C_xpyrH]⁺. Anions: dicyanamide, [N(CN)₂]⁻; hexafluorophosphate, [PF₆]⁻; tetrafluoroborate, [BF₄]⁻; bis(trifluoromethanesulfonyl)imide, [N(SO₂CF₃)₂]⁻ or [NTf₂]⁻; trifluoromethanesulfonate or triflate, [CF₃SO₃]⁻ or [OTf]⁻; nitrate, [NO₃]⁻; carboxylate [RCOO]⁻; hydrogen sulfate [HSO₄]⁻. Abbreviations: AIL, aprotic ionic liquid; IL, ionic liquid; PIL, protic ionic liquid; R, alkyl chain.

1.1.2. Protic ionic liquids.

Protic ionic liquids (PILs) are formed through the transfer of a proton from a Brønsted acid (HA) to a Brønsted base (B):



By definition, they contain dissociable (acidic) protons and possess intrinsic (anhydrous) proton conductivity. The proton activity in PILs depends on the identity of the constituent Brønsted acid/base, analogous to pH in aqueous systems, which allows some control over proton-coupled chemical/electrochemical processes (19–26).

When complete transfer of the proton from HA to B occurs, the properties of PILs are generally not discernible from those of AILs. This is often the case when HA is a strong acid and B is a strong base in aqueous media, for example, when triflic acid is combined with a tertiary

amine. When proton transfer from HA to B does not go to completion, the melt may contain a significant amount of neutral species (i.e., HA/B). This is often the case when HA is a weak aqueous acid and/or B is a weak aqueous base, for example, when a carboxylic acid is combined with imidazole or pyridine. Proton-donor (i.e., HA or BH^+) and -acceptor (i.e., B or A^-) sites establish a hydrogen-bonded cation/anion network, often resulting in water-like properties (23, 25). In addition, when the proton transfer is reversible (does not go to completion), the boiling temperature of $[\text{BH}][\text{A}]$ can be below its decomposition temperature, thereby allowing the PIL to be distilled (23, 27, 28). The names, abbreviations, and structures of commonly encountered PIL cations and anions are also provided in Figure 1.

1.2. Physicochemical Properties of Ionic Liquids

One attractive feature of ILs is their great versatility; it has been estimated that 10^{18} different ILs could be prepared by varying the constituent anion and cation (3). Indeed, they are commonly referred to as designer solvents because their physicochemical properties can be tuned to an extent by changing their constituent cation and/or anion. Although the only truly ubiquitous property shared by all ILs is intrinsic ionic conductivity, in the chemical literature, they are often claimed to possess a number of generic properties. These include variable degrees of water miscibility (hydrophobicity/hydrophilicity); high viscosity (usually in the range of 20 to 1,000 cP); negligible vapor pressure and nonflammability; high solvating ability, but low or no coordinating ability; high thermal, chemical, and electrochemical stability; large liquidus range; and they are nontoxic/environmentally friendly (1, 3, 7, 16, 29–31). In reality, the actual physicochemical properties of an IL are decided by the identity of its constituent cation and anion, and although some ILs do possess some of the above attributes, there are many exceptions (5, 30). The focus herein is the specific use of ILs as nonconventional electrolytes in electrochemical investigations, whereby the IL simultaneously functions as the solvent and salt (1, 32), with an emphasis on the energetics (thermodynamics) of proton transfer (i.e., minus logarithm of acidity equilibrium constant, K_a , known as $\text{p}K_a$) and electrode reaction mechanisms of the H^+/H_2 process.

2. PROTON TRANSFER IN IONIC LIQUID MEDIA

Proton (H^+) transfer is involved with many of the most important reactions in biology and chemistry (33, 34). For example, proton transfer and conduction play an important role in green energy conversion technologies, such as electrochemical CO_2 fixation (electro-reduction) (28, 35, 36), methanol oxidation (37), and water (photo)electrolysis (38). As alluded to above, air/water stable (nonhaloaluminate) ILs, particularly PILs, have been identified as potential anhydrous proton conductors, which could be employed at temperatures well above $100^\circ C$ (23, 39). Indeed, there are many applications in areas as broad as energy conversion and storage (e.g., proton-exchange membrane fuel cells, PEMFCs) (12, 13, 39–42), synthetic chemistry (e.g., hydrogenation/dehydrogenation) (8, 9), separations chemistry (15), and electrochemistry (e.g., electrochemical hydrogenation, gas sensors) (43) that would benefit from high-temperature, anhydrous proton conduction. A general discussion on the energetics (thermodynamics) of proton transfer is included below, followed by a summary highlighting recent electrochemical studies on the pK_a scale in IL media.

2.1. Equilibrium Acidity

The acid dissociation constant (K_a) of a Brønsted acid, HA, formally defined as follows, is a quantitative measure of acid strength in solution:



where H^+ is taken to be a solvated proton species (vide infra). Although the acid is taken to be a neutral species (HA) in Equation 2, the expression for K_a is equally valid for a cationic acid species, BH^+ (i.e., a protonated neutral base, B):



It should be noted that, while the theory discussed herein refers to either HA or BH^+ (or HA/H_2 or BH^+/H_2 couples, respectively; see below) as the weak acid, it is equally applicable for both species. Brønsted acidity/basicity is a well-established concept in aqueous media (44), where water, an amphoteric species, can act as a Brønsted base and accept a proton:



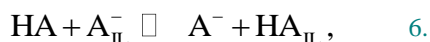
or it can act as a Brønsted acid and donate a proton:



From Equation 4, it is clear that the hydronium ion (also known as a hydrated/solvated proton), H_3O^+ , is the strongest acid that can exist in aqueous media. In other words, the process shown in Equation 4 effectively levels the acidity of all strong acids in aqueous media and is the origin of the aqueous $\text{p}K_{\text{a}}$ scale (45, 46), where $\text{p}K_{\text{a}} = -\log_{10}K_{\text{a}}$.

Many organic compounds contain acidic and/or basic functional groups that dictate their physical, chemical, and biological properties. Indeed, bond transformations in solution frequently involve the cleavage or formation of R–H bonds. As described above, $\text{p}K_{\text{a}}$ describes the free energy change of R–H bond heterolysis, making it a critically important thermodynamic parameter in synthetic chemistry and related fields (47–49). Equilibrium acidities ($\text{p}K_{\text{a}}$) are media dependent, being dictated by the ability of the solvent to solvate each of the species outlined in Equation 2 (i.e., HA, A^- , and H^+) or Equation 3 (i.e., BH^+ , B, and H^+). It follows that solvent acidity/basicity, dielectric properties, and the ability to donate/accept hydrogen bonds can all influence the $\text{p}K_{\text{a}}$ value of an acid in solution (49, 50). Although $\text{p}K_{\text{a}}$ data are most readily available in water (51, 52), $\text{p}K_{\text{a}}$ scales have been established in a range of nonaqueous solvents, including acetonitrile (53), dimethylsulfoxide (49, 54, 55), and 1,2-dichloroethane (53). A variety of methods (56) are typically employed to quantify $\text{p}K_{\text{a}}$ in conventional media, including potentiometry (57), spectrophotometry (49, 58), and voltammetry (50, 54, 55).

The protons released from the dissociation of a Brønsted acid in IL media must associate with (or be solvated by) the most basic component of the IL, most commonly the anion (A_{IL}^-):



where HA_{IL} is the strongest acid that may exist in a given IL. HA_{IL} effectively levels the acidity of strong acids in IL media, comparable to H_3O^+ in aqueous media. In other words, HA_{IL} is the origin of the $\text{p}K_{\text{a}}$ scale in IL media, and for this reason, $\text{p}K_{\text{a}}$ data are not directly comparable for ILs with different constituent anions (45, 47, 48, 59–61). It should be noted that from this point

forward, H^+ refers to the solvated proton species and is equivalent to HA_{IL} in the context of ILs or H_3O^+ in the context of aqueous media.

2.2. The $\text{p}K_{\text{a}}$ Scale in Ionic Liquids

Although electrochemical (voltammetric) studies are the main focus herein, the recent comprehensive work by Cheng and coworkers should be acknowledged (47, 48, 62, 63). Using a spectrophotometric (overlapping indicator) method, these authors have established the equilibrium acidity of over 75 different acids (e.g., carbon acids, oxyacids, protonated amines, and sulfonamides) in a range of ILs. In all studies, $\text{p}K_{\text{a}}$ (IL) data have been correlated to corresponding $\text{p}K_{\text{a}}$ data available in molecular solvents (e.g., water, dimethylsulfoxide, and acetonitrile) and the gas phase (where available), to draw conclusions about the relative solvating properties (i.e., Lewis acidity/basicity) of ILs. In addition, in all studies it is noted that the identity of both the IL anion, and to a lesser extent, the cation was found to influence the $\text{p}K_{\text{a}}$ of a given acid, as discussed further below.

The Angell group (24) first explored the concept of $\text{p}K_{\text{a}}$ (proton thermodynamics) in the electrochemical context by studying hydrogen redox chemistry (i.e., the H^+/H_2 process, described below) at a platinum (Pt) electrode in 10 PILs of widely varying proton transfer energies. A significant gap (ca. 0–800 mV) between the onset potential at which the hydrogen evolution reaction (HER) occurs and the potential at which the hydrogen oxidation reaction (HOR) occurs facilely was observed. This difference occurs because hydrogen oxidation involves the HA/H_2 couple, whereas proton reduction involves the BH^+/H_2 couple. It follows that the potential gap separating these two processes is proportional to the energetics for proton extraction from the protonated anion (i.e., HA in Equation 1) relative to the cation (i.e., BH^+ in Equation 1), which is defined by the differences in proton free energy between the Brønsted couples HA/A^- and BH^+/B . Hence, the potential difference between the HA/H_2 (HOR) and BH^+/H_2 (HER) can be correlated to the difference between the aqueous $\text{p}K_{\text{a}}$ values of HA and BH^+ (i.e., $\Delta\text{p}K_{\text{a}}$), suggesting that aqueous $\Delta\text{p}K_{\text{a}}$ data provide a good approximation to proton activity in PILs.

Kanzaki and coworkers (64, 65) recently established a $\text{p}K_{\text{a}}$ scale (14 $\text{p}K_{\text{a}}$ values from 12 compounds) in the neat PIL ethylammonium nitrate (EAN), which was determined using potentiometric titration. $\text{p}K_{\text{a}}(\text{EAN})$ values were consistently one unit greater than the corresponding value in water, regardless of the structure, charge (neutral, cationic, and anionic

acids were investigated), and/or hydrophobicity of the compounds. The authors attributed this to the stronger acidity of HNO₃ (i.e., HA_{IL} or H⁺; see Equation 6) in EAN than that of H₃O⁺ in water, rather than a difference in the solvation state of the ions. In addition, assuming that pK_a(EAN) = pK_a(H₂O) + 1 always applies, and from the autoprotolysis constant of EAN [pK_{AP} = 9.83, determined in a previous study (66)], it was concluded EAN is a solvent with stronger acidity and weaker basicity (approximately 10⁵ times weaker) than water. Furthermore, although not based on thermodynamically rigorous arguments, it was estimated that the pH scale in EAN lies in the range of –1 to 9 on the water-based pH scale, again suggesting that EAN is an acidic solvent relative to aqueous media.

The pK_a values of weak acids dissolved in an IL can be conveniently calculated using dynamic electrochemical methods such as cyclic voltammetry from the following relationship (45, 50, 54, 55, 67):

$$E^{0'}(\text{BH}^+ / \text{H}_2) - E^{0'}(\text{H}^+ / \text{H}_2) = \frac{RT}{F} \ln \frac{[\text{B}][\text{H}^+]}{[\text{BH}^+]} = -\frac{2.303RT}{F} \text{p}K_a, \quad 7.$$

where $E^{0'}(\text{H}^+/\text{H}_2)$ and $E^{0'}(\text{BH}^+/\text{H}_2)$ are the formal reversible potentials for the H⁺/H₂ and BH⁺/H₂ processes (discussed below), respectively. R is the universal gas constant, T is the absolute temperature, and F is Faraday's constant. Indeed, this method was used by Barhdadi et al. (45) to estimate the pK_a value of the pyridinium cation in a range of ILs, where they reported a strong dependence on the identity of the IL anion. In their study, it was assumed that $E_{1/2} \approx E^{0'}$, where $E_{1/2}$ is the reversible half-wave potential, introduced originally as a polarographic term, but in the present context taken to be the average of the reductive ($E_{\text{p,red}}$) and oxidative ($E_{\text{p,ox}}$) peak potentials of a reversible transient cyclic voltammogram (the midpoint potential, E_{mid}) (55, 68). Although this approximation is valid for simple (unimolecular) reactions in conventional media (equations describing the relationship between $E^{0'}$, $E_{1/2}$ and E_{mid} can be found in 67, 68), the bimolecular nature of the H⁺/H₂ process and grossly different diffusion coefficients of H⁺ and H₂ in IL media mean that this approximation introduces considerable systematic error into the determination of pK_a (vide infra).

Building on this work, our group (59–61) reported a series of studies focusing on the energetics (thermodynamics) of proton transfer in IL media, predominantly AILs, which were probed using electrochemical (voltammetric) methods. Pt was selected as the electrode, as the

H^+/H_2 and BH^+/H_2 (or HA/H_2) processes are well defined and chemically reversible on this material. This allows for the accurate estimation of $E_{1/2}$, which can be used to derive pK_a values, as described in detail below. In the first study, the nature of the solvated proton species (i.e., HA_{IL} ; see Equation 6) was investigated in a range of AILs: $[C_2mim]^+$, $[C_4mpyr]^+$, $[S_{2,2,2}]^+$, $[C_4dmim]^+$, $[N_{1,1,2,3}]^+$, and $[N_{1,4,4,4}]^+$, each with the common $[NTf_2]^-$ anion ($H[NTf_2]$ was the proton source). Through correlation of the electrochemically derived proton diffusion coefficient [calculated using the convolution method (69–71) or through chronoamperometry (72)] with the self-diffusion coefficient of $[NTf_2]^-$ (derived using pulsed field gradient spin-echo nuclear magnetic resonance), it was unequivocally shown that H^+ remains associated with the anion part of the IL, and the strongest acid that can possibly exist in an $[NTf_2]^-$ IL is therefore $H[NTf_2]$ (45). In other words, $H[NTf_2]$ is the origin of the pK_a scale in $[NTf_2]^-$ media, in accordance with the concepts outlined above.

This initial work shows that identity of the cation has very little influence on E^0 (H^+/H_2), which is a measure of the energetics of proton transfer in this medium, with the H^+/H_2 process occurring at approximately -0.030 V versus ferrocene/ferrocenium (Fc/Fc^+) in all investigated $[NTf_2]^-$ AILs [it was assumed that the Fc/Fc^+ couple possesses a solvent-independent formal potential (73–75)]. In a subsequent study (60), it was shown that E^0 (H^+/H_2) is strongly governed by the anion of the IL. For example, a value of approximately -0.34 V versus Fc/Fc^+ was obtained in $[C_2mim][OTf]$ [H^+ was from either $H[OTf]$ or $H[NTf_2]$, both strong acids in this media]. In contrast, two proton reduction processes were found in the PIL $[N_{H,2,2,2}][NTf_2]$; one occurred at approximately -0.030 V versus Fc/Fc^+ , corresponding to the $H[NTf_2]/H_2$ process (as above for the AILs), and one occurred at approximately -0.9 V versus Fc/Fc^+ , originating from the bulk reduction of the protonated PIL cation [i.e., the $(N_{H,2,2,2})^+/H_2$ process].

In later studies (60, 61), the pK_a of a range of NH [protonated amines and sulfonamides (60)] and OH [phenols, carboxylic acids and sulfonic acids (61)] acids were quantified in $[C_2mim][NTf_2]$. Building on the theory reported by Barhdadi et al. (45), the following relationships between E^0 and $E_{1/2}$ were derived using the diffusion layer approximation method (55, 67, 76, 77):

$$E^0(H^+/H_2) = E_{1/2}(H^+/H_2) - \frac{RT}{2F} \ln \left(\frac{\sqrt{D_{H_2}}}{\sqrt{D_{H^+}}} \right) - \frac{RT}{2F} \ln [H^+], \quad 8.$$

$$E^{0'}(\text{BH}^+ / \text{H}_2) = E_{1/2}(\text{BH}^+ / \text{H}_2) - \frac{RT}{2F} \ln \left(\frac{4\sqrt{D_{\text{H}_2}}}{\sqrt{D_{\text{BH}^+}}} \right) + \frac{RT}{2F} \ln [\text{BH}^+], \quad 9.$$

where D is the diffusivity (diffusion coefficient). Combining Equations 7 to 9 gives

$$-\frac{2.303RT}{F} \text{p}K_{\text{a}} = E_{1/2}(\text{BH}^+ / \text{H}_2) - E_{1/2}(\text{H}^+ / \text{H}_2) + \frac{RT}{2F} \ln \left(\frac{\sqrt{D_{\text{BH}^+}}}{\sqrt{D_{\text{H}^+}}} \right) + \frac{RT}{2F} \ln \left[\frac{(\text{BH}^+)(\text{H}^+)}{4} \right]. \quad 10.$$

Note that in the derivation of Equations 9 and 10, it was assumed that $D_{\text{B}} = D_{\text{BH}^+}$. As alluded to above, assuming that $E_{1/2} \approx E^{0'}$ neglects the two logarithmic terms shown in Equation 10, which leads to considerable systematic error (approximately 3 $\text{p}K_{\text{a}}$ units when working at millimolar concentrations) in the determination of $\text{p}K_{\text{a}}$. As highlighted above, $E_{1/2}$ values can be directly estimated from a cyclic or derivative cyclic voltammogram from the average of $E_{\text{p,red}}$ and $E_{\text{p,ox}}$ (i.e., E_{mid}), and D values can be derived electrochemically using the convolution method (69–71) or chronoamperometry (72). Indeed, it was demonstrated how all of the parameters required to calculate $\text{p}K_{\text{a}}$ from Equation 10 could be derived from an IL solution containing a 2:1 mixture of H^+ and B, as illustrated in Figure 2 for $\text{H}[\text{NTf}_2]$ and pyridine in $[\text{C}_2\text{mim}][\text{NTf}_2]$. It was also shown how the homoassociation constant (K_{homo}) could be derived voltammetrically for the carboxylic and sulfonic acids (vide infra) (61).

<COMP: PLEASE INSERT FIGURE 2 HERE>

Figure 2 (a) A cyclic voltammogram obtained from the reduction of 57.4 mM $\text{H}[\text{NTf}_2]$ and 24.3 mM pyridine in $[\text{C}_2\text{mim}][\text{NTf}_2]$ at a 1.6-mm-diameter Pt macrodisk electrode with a scan rate of 100 mV s^{-1} . The $E_{1/2}$ values used in Equation 10 are calculated as follows: $E_{1/2} \approx E_{\text{mid}} = (E_{\text{p,ox}} + E_{\text{p,red}})/2$. (b) Experimental (lines) and Shoup-Szabo theoretical chronoamperograms (circles) obtained from the solution used in panel a at a 20- μm diameter Pt microdisk electrode by (i) stepping the potential to -0.323 V versus Fc/Fc^+ (blue trace), (ii) stepping the potential to -1.023 V versus Fc/Fc^+ (purple trace), and (iii) subtracting curve i from curve ii (red trace). The D values used in Equation 10 are obtained from the Shoup-Szabo fitting procedure. Abbreviation: Fc/Fc^+ , ferrocene/ferrocenium. Adapted with permission from Reference 60. Copyright 2015, American Chemical Society.

Using the approach outlined above, the $\text{p}K_{\text{a}}$ values of 20 weak acids, covering 18 orders of magnitude in acid strength ($2.0 \leq \text{p}K_{\text{a}} \leq 19.5$), were calculated and compared with data from

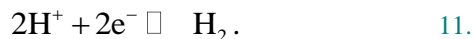
conventional solvents (acetonitrile, AN, and water, shown in **Figure 3a** and **3b**, respectively), to gain insight into how the nature of the solvent [i.e., dielectric properties, Lewis acidity/basicity, hydrogen donating/accepting ability, etc. (18, 78)] influences equilibrium acidity. As shown in **Figure 3a**, with the exception of H[OTf], the $pK_a(\text{IL})$ data correlate well with $pK_a(\text{AN})$, with pK_a values consistently 1–2 units lower in [C₂mim]NTf₂] compared to AN. On the other hand, as shown in **Figure 3b**, considering all of the acids in a single group, $pK_a(\text{IL})$ data correlate poorly with $pK_a(\text{H}_2\text{O})$, although pK_a values in [C₂mim][NTf₂] are consistently several units higher than in H₂O, owing to the exceptionally high dielectric constant and Gutmann donor/acceptor numbers of the latter solvent. Dividing the acids into two groups, cationic and neutral, makes it clear that there is good correlation between $pK_a(\text{aq})$ and $pK_a(\text{IL})$ for acids of like charge (i.e., cationic versus cationic or neutral versus neutral) but not for acids of different charge (i.e., cationic versus neutral). This phenomenon was explained by the well-known preferential solvation of the water molecule toward oxyanions through hydrogen bonding (i.e., the acidity of neutral oxyacids are enhanced relative to protonated amines in aqueous media), which is absent in the neat, poorly hydrogen-bonding AIL. Finally, it was shown how the nature of the IL can have a significant influence on the acid/base properties of a given weak acid; taking tosylic acid as an example, it was shown that switching the cationic constituent from [C₂mim]⁺, a poor hydrogen bond donor, to [N_{H,2,2,2}]⁺, a good hydrogen bond donor, suppresses anionic homoassociation (discussed below) and increases the acidity of this weak acid a thousandfold (i.e., pK_a decreases from 6.2 to 3.3) (60, 61).

<COMP: PLEASE INSERT FIGURE 3 HERE>

Figure 3 (a) Plot of $pK_a(\text{AN})$ versus $pK_a(\text{IL})$ for a range of weak neutral acids. (b) Plot of $pK_a(\text{aq})$ versus $pK_a(\text{IL})$ for a range of nitrogen (*triangles*) and oxygen (*squares*) acids. Regression lines for the uncharged (*red*) and charged (*purple*) acids have been included solely to guide the reader's eye. H[OTf] not considered when calculating the regression line in panel a. Abbreviations: AN, acetonitrile; An, aniline; aq, aqueous media; ClPyr, 2-chloropyridine; DBSA, di(benzenesulfonyl)imide; DCAA, dichloroacetic acid; dClPyr, 2,4-dichloropyridine; GA, glycolic acid; H[OTf], triflic acid; H[OTs], tosylic acid; IL, ionic liquid; MA, malonic acid; MeIm, *N*-methylimidazole; MePyr, *N*-methylpyrrolidine; MSA, methanesulfonic acid; oHBA, *o*-hydroxybenzoic acid; oPD, *o*-phenylenediamine; PCP, pentachlorophenol; Pyr, pyridine; SACC, saccharin; TCAA, trichloroacetic acid. Adapted with permission from Reference 61. Copyright 2015, American Chemical Society.

3. THE H⁺/H₂ PROCESS IN IONIC LIQUIDS

The HER and HOR are technologically important processes (e.g., in electrolyzers and fuel cells, respectively) that have been characterized on many electrode materials in a range of media (79–81), predominantly aqueous (76, 82, 83):

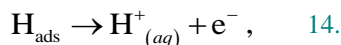
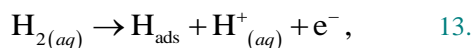
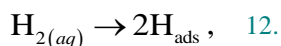


In addition, the fundamental reference potential scale in aqueous electrochemistry, the standard hydrogen electrode, is based on the H⁺/H₂ couple (67). Although Equation 11 is an apparently simple one electron per proton process, it is subject to significant kinetic barriers, necessitating the use of an electrocatalyst in practical (industrial) applications. It follows that different metal electrodes are well known to exhibit vastly different catalytic activities toward the HER/HOR in aqueous media (84, 85).

As mentioned above, ILs—particularly PILs—have attracted significant interest as anhydrous proton conductors for application in nonhumidified intermediate temperature fuel cells (12, 27, 31). In the past decade, numerous studies have been dedicated to identifying PIL formulations that display fast proton transport in addition to facile HOR and oxygen reduction reaction (ORR) kinetics (12, 22, 24, 25, 39–41). These studies have been addressed in a number of recent comprehensive reviews (12, 26, 42). Application-driven studies on the HER/HOR in IL media are not discussed here. Rather, recent fundamental studies on the mechanistic aspects of the H⁺/H₂ process in IL media are reviewed.

3.1. The Hydrogen Oxidation Reaction

The HOR is postulated to proceed via the Tafel-Heyrovsky-Volmer route in acidic aqueous media (80, 82, 86):



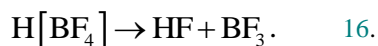
where H_{ads} is a chemisorbed hydrogen atom. Thus, the formation of H_{ads} through dissociative chemisorption (Tafel reaction; Equation 12) or dissociative chemisorption and ionization to H⁺

(Heyrovsky reaction; Equation 13) is followed by the oxidation of H_{ads} (Volmer reaction; Equation 14) to form H^+ .

Compton and coworkers (87, 88) performed the pioneering work on the mechanistic aspects of the HOR in IL media. In their first reports, the HOR was investigated in a range of AILs. On Pt, a broad (i.e., large cyclic voltammetric peak-to-peak separation, ΔE_p) but chemically reversible process was observed in the $[NTf_2]^-$ and $[OTf]^-$ ILs, which the authors attributed to the following process:



The HOR is inhibited at strongly oxidative potentials [also observed in the study by Angell and coworkers (24), described above], which is attributed to blocking of the catalytically active sites on the Pt electrode surface by a platinum oxide (PtO_x) layer (i.e., the electrode is passivated), formed due to the presence of residual water in the IL. It was also shown that if the Pt electrode is preanodized at strongly oxidizing potentials, the kinetics of the HOR are greatly increased in the potential range where the surface oxide is not present (evidenced by a decreased ΔE_p), presumably due to the formation of a catalytically active pristine Pt surface after PtO_x formation/dissolution. In $[BF_4]^-$, $[PF_6]^-$, Cl^- , and $[NO_3]^-$ ILs, the HOR is only partially chemically reversible, which the authors attributed to instability of the protonated anion (formed during the HOR; see Equation 15). In the case of $[PF_6]^-$ and $[BF_4]^-$, it is thought that the anion undergoes acid-catalyzed dissociation (decomposition) on the voltammetric timescale, for example:



In the case of Cl^- , it is thought that HCl (formed from hydrogen oxidation; see Equation 15) reacts to form stable $H[Cl_2]^-$, as highlighted in a first principles simulation study by Del Popolo et al. (89). An analogous mechanism was also proposed for $[NO_3]^-$.

The identity of the IL anion, and to a lesser degree the IL cation, can have a significant influence on the kinetics of the HER/HOR, as proposed by Navarro-Suárez and coworkers (90), who investigated the HOR at Pt (100), Pt (110) and Pt (111) macroelectrodes (flame annealed, low-index Pt single crystals) in a range of imidazolium-based AILs. The activity toward the HOR (assessed from the onset potential of the HOR) was shown to increase in the order of Pt

(100) < Pt (110) < Pt (111) in [C₄mim][OTf], [C₂mim][EtSO₄], and [C₄mim][BF₄], whereas Pt (100) was found to be the most active surface in [C₂mim][NTf₂]. The variations in electrocatalytic activity of low-index Pt crystal surfaces were attributed to differences in anion adsorption at oxidative potentials (specifically, weaker adsorption at more densely packed surfaces leads to higher activity). In a recent study, Tang et al. (91) proposed that the HOR is catalyzed by the formation of Pt-bound NTf₂• radicals in deaerated [C₄mpyr][NTf₂], a conclusion supported by experimental data (cyclic voltammetry) and density functional theory calculations.

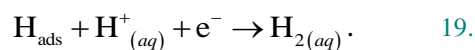
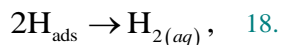
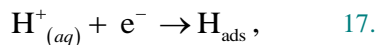
The Walsh group (92) investigated the HOR at a polycrystalline Pt rotating disk electrode in the PIL [N_{H,1,2,2}][OTf]. This reaction was found to become hindered at highly positive (oxidizing) potentials. This feature was shown by X-ray photoelectron spectroscopy to be attributable to the formation of a blocking PtO_x layer, effectively passivating the electrode to the electrocatalytic process, which is in agreement with the earlier work by Angell's group (24) and Compton's group (87, 88). In a follow-up study (93), the role of adsorption in the electrocatalytic HER was investigated in a more extensive range of PILs, [N_{H,1,2,2}][OTf], [N_{H,1,1,2}][OTf], and [N_{H,1,2,2}][NTf₂]. Voltammetric analysis revealed that a monolayer of hydrogen adsorbs (H_{ads}; see Equations 12–14) onto Pt during potential cycling in the [OTf][−] PILs but not the [NTf₂][−] one. The authors attributed the suppression of H_{ads} formation in the latter class of PIL to the adsorption of the [NTf₂][−] anion onto the electrode surface at relatively low oxidative potentials (i.e., blockage of catalytic sites by adsorbed [NTf₂][−]).

The Walsh group (94) has also probed the HOR in [N_{H,1,2,2}][OTf] under high mass transport conditions using hydrodynamic and ultramicroelectrode voltammetry. Whereas only a single, mass transport–limited HOR plateau is observed at a Pt rotating disk electrode, an additional plateau was detected when using a Pt ultramicroelectrode (i.e., the voltammetric wave is split into two processes), which resulted from the higher rates of mass transport achievable at the latter type of electrode. On this basis, three models were proposed to fit the experimental data. Two are based on the coexistence of dual reaction pathways (e.g., Volmer-Tafel versus Heyrovsky-Volmer are dominant in different potential regions; see Equations 12 to 14), and a third is based on the premise that underpotential deposited hydrogen atoms (H_{UPD}) can block the further adsorption and oxidation of H₂ at the Pt surface. Despite reasonably satisfactory theory-experimental fits for all three models, the H_{UPD}-blocking model best described the responses,

leading to the conclusion that H_{UPD} can act as a blocking species during electrocatalytic reactions in PIL media.

3.2. The Hydrogen Evolution Reaction

The HER is postulated to proceed via the Volmer reaction (Equation 17), followed by either the Tafel (Equation 18) or Heyrovsky (Equation 19) reaction in acidic aqueous media (80, 82, 86):



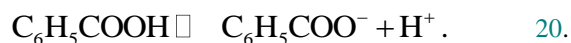
Thus, the formation of H_{ads} on the electrode surface by electron transfer (reduction) is followed by either surface migration and dimerization of H_{ads} to form H_2 or the direct formation of H_2 from H_{ads} and H^+ (solution) by electron transfer. The preferred reaction pathway depends on the identity of the metallic electrode and is thought to be governed by whether Equation 17 is sluggish or facile relative to H_{ads} migration across the electrode surface (80).

The Compton group (95) has investigated the HER from $H[NTf_2]$ or HCl as the proton source in $[C_4mim][NTf_2]$. A chemically reversible proton reduction process is observed on Pt, which is thought to proceed via the combination of reactions outlined in Equations 17 to 19. On Au, the HER occurs (chemically) irreversibly at potentials negative of those on Pt, whereas on glassy carbon (GC), an irreversible, broad reduction process is observed at even more negative potentials and just prior to solvent breakdown. These results are in accordance with the relative order of hydrogen overpotentials of the electrode materials in aqueous media: $GC \gg Au > Pt$. On Pt, proton reduction from HCl is chemically reversible, occurring at potentials negative of the $H[NTf_2]/H_2$ process, in accordance with the relative acidities of HCl and $H[NTf_2]$ (vide supra). These authors also postulate that $H[Cl_2]^-$ forms as an intermediate during proton reduction at potentials where the concentrations of both HCl and Cl^- are significant.

In later studies, the Compton group (80, 96) investigated proton reduction (from $H[NTf_2]$ as the proton source) on a range of metallic electrodes (Au, Mo, Ni, Ti, and Pt) in $[C_2mim][NTf_2]$ [and with an expanded range of ILs in a follow-up study (81)]. Chemically and electrochemically irreversible proton reduction was observed on all of the metal surfaces except Pt, with no H_2

process being observed on the reverse cyclic voltammetric sweep within the investigated potential range. The charge-transfer coefficient (α) was found to be ≤ 0.5 on all metal surfaces (determined through mass transport corrected Tafel slope analysis), indicating that the Volmer reaction (Equation 17) is the rate-determining step in all cases. Finally, the heterogeneous kinetics of the HER (estimated by numerical simulation) was found to be strongly dependent on the identity of the metallic electrode, with the electrocatalytic trend being $\text{Pt} > \text{Mo} > \text{Au} > \text{Ni} > \text{Ti}$, which is different to that established in aqueous media: $\text{Pt} > \text{Ni} > \text{Au} > \text{Mo} > \text{Ti}$.

Compton and coworkers (97–99) have also investigated the proton reduction process from the weak aqueous acid, benzoic acid, on a Pt electrode in a range of ILs. Proton reduction from benzoic acid (i.e., the HA/H_2 process) occurred at potentials negative of the H^+/H_2 process (i.e., solvated proton reduction) and was postulated to proceed via a generic CE mechanism, where the electron transfer step (E; see Equations 11, 17–19) is preceded by a fast chemical (dissociation) step (C):



A reductive prepeak was observed prior to the main reduction peak in all ILs examined, which was assigned to the formation of adsorbed H^\bullet on the Pt electrode surface. The potential region in which proton reduction from benzoic acid occurs was also found to be dependent on the identity of the IL anion, consistent with earlier reports (81, 87, 88).

Our group (59) recently investigated the mechanism of the HER with $\text{H}[\text{NTf}_2]$ as the proton source in a range of AILs ($[\text{C}_2\text{mim}]^+$, $[\text{C}_4\text{mpyr}]^+$, $[\text{S}_{2,2,2}]^+$, $[\text{C}_4\text{dmim}]^+$, $[\text{N}_{1,1,2,3}]^+$, $[\text{N}_{1,4,4,4}]^+$, each with the common $[\text{NTf}_2]^-$ anion) by combining experimental cyclic voltammetric data at a Pt electrode with that from computational simulations. In this investigation, it was found that the voltammetric response was very sensitive to the history of the Pt electrode (i.e., cleanliness/surface state). As shown in Figure 4a, after the electrode has been freshly polished (cycle 1), a well-defined reductive response is obtained, which noticeably degrades on cycling the potential (or by leaving the electrode submerged in the IL at the open circuit potential), becoming flattened and less peak shaped (i.e., the electrode becomes deactivated). As demonstrated in Figure 4b, the initial voltammetric response can be recovered by mechanically polishing the electrode or by electrochemical conditioning at oxidative potentials (anodic polarization). In other words, when the oxidative limit is extended to 2.2 V (versus Fc/Fc^+), the

initially degraded response improves with cycling, indicating that the electrode is activated at oxidative potentials [previously reported in both conventional solvents (79) and other ILs (88)]. In a later study, it was shown that the degradation of the voltammetric HER response occurred more rapidly in [C₂mim][OTf], suggesting that electrode deactivation is intrinsically linked to the IL anion (60).

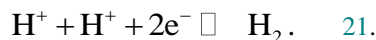
<COMP: PLEASE INSERT FIGURE 4 HERE>

Figure 4 Cyclic voltammograms obtained from the hydrogen evolution reaction (proton source = H[NTf₂]) in [C₂mim][NTf₂] at a 20-μm-diameter Pt microdisk electrode. (a) Ten cycles ($\nu = 100 \text{ mV s}^{-1}$) in the potential range 0.41 to -0.59 V (versus Fc/Fc⁺) demonstrate progressive deactivation of the electrode. (b) Four cycles ($\nu = 100 \text{ mV s}^{-1}$) in the potential range of 2.21 to -0.59 V (versus Fc/Fc⁺) demonstrate the activation of the electrode with anodic polarization. (c) Cyclic voltammograms obtained with $[\text{H}^+] = 99.2 \text{ mM}$ and $\nu = 50, 100, 250,$ and 500 mV s^{-1} . (d) Cyclic voltammograms obtained with $\nu = 100 \text{ mV s}^{-1}$ and $[\text{H}^+] = 25.4, 44.5, 75.8,$ and 99.2 mM . Simulated cyclic voltammograms (*circles*) are also shown in panels c and d, obtained by combining Equations 22 and 23 with the following parameters: $E^0(\text{H}^+/\text{H}^*) = -0.148 \text{ V}$, $k_s = 0.022 \text{ cm s}^{-1}$, $\alpha = 0.50$ (Equation 22, apparent values); $K_{\text{dim}} = 10^4$, $k_{\text{dim}} = 10^{16} \text{ M}^{-1} \text{ s}^{-1}$ (Equation 23); $D_{\text{H}^+} = 3.1 \times 10^{-7} \text{ cm}^2 \text{ s}^{-1}$, $D_{\text{H}_2} = 2.2 \times 10^{-5} \text{ cm}^2 \text{ s}^{-1}$. $E^0(\text{H}^+/\text{H}_2) = -0.030 \text{ V}$, derived from $E^0(\text{H}^+/\text{H}^*)$ and K_{dim} . Abbreviations: Fc/Fc⁺, ferrocene/ferrocenium; IL, ionic liquid; PtO_x, platinum oxide; UPD, underpotential deposited. Adapted with permission from Reference 59. Copyright 2014, American Chemical Society.

Figure 4c,d shows representative cyclic voltammograms obtained at a 20-μm-diameter Pt microdisk electrode, which had previously been activated by stepping the potential to $\approx 2 \text{ V}$ versus Fc/Fc⁺ for $\leq 1 \text{ ms}$. D_{H^+} ($\sim 10^{-7} \text{ cm}^2 \text{ s}^{-1}$) and D_{H_2} ($\sim 10^{-5} \text{ cm}^2 \text{ s}^{-1}$) are hundredfold different in this medium, and as a result, the reduction (HER) and oxidation (HOR) processes are peak shaped (mass transport due to both planar and radial diffusion) and sigmoidal (mass-transport predominantly due to radial diffusion), respectively. The underpotential deposition of adsorbed hydrogen on the electrode is observed prior to the main reduction process (labeled in **Figure 4c,d**), consistent with the behavior of Pt surfaces in aqueous acidic media (82).

Also shown in **Figure 4c,d** are simulations of the voltammetric response. Although in reality, adsorption is thought to play an important role in the HER and HOR (80, 82, 86), for simplicity, the H^+/H_2 reaction has been treated as a purely solution based process, simulated using the DigiElch electrochemical simulation software (<http://www.elchsoft.com/digielch/DigiElch7/>).

A single step process, using the bimolecular capability of DigiElch (version 7) was initially considered:



However, this was not found to emulate the experimental data over a wide range of conditions, requiring a different set of parameters for each investigated concentration or scan rate. Building on this, two mechanisms were considered, based on the Volmer-Tafel (Equations 17 and 18) and Volmer-Heyrovsky (Equations 17 and 19) routes, both of which were both found to give excellent agreement with the experimental data:



where E^0 , k_s , and α are the formal potential, standard heterogeneous electron-transfer rate constant at E^0 and charge transfer coefficient, respectively. As the Volmer-Tafel (Equations 22 and 23) route is the simpler mechanism from a simulation perspective (54, 55, 59, 60), it is solely considered herein. As discussed above, in reality, H^* is likely to be a surface-confined species (82, 83), although for simplicity it has been treated as a solution-based (diffusing) species in the simulations. One consequence of treatment of the mechanism in this manner is that the process shown in Equation 23 can be regarded as empirically based, as are the parameters k_s , α , K_{dim} , k_{dim} , and D_{H^*} (i.e., they are not physically meaningful) (54). Furthermore, it should be emphasized that the kinetic parameters, k_s , and α , are apparent values and therefore should not be interpreted quantitatively.

Despite the use of a significantly simplified mechanism, the simulations are in excellent agreement with the experimental data in all investigated ILs over a wide range of scan rates (Figure 4c) and concentrations (Figure 4d). Regardless of the mechanism employed (i.e., Equations 22 and 23 in Figure 4 or Equations 22 and 24 in 59), the first electron transfer step (Volmer reaction, Equation 17) is assumed to be rate determining on Pt (i.e., k_{dim} , or $k_{s,2}$ were set to be fully reversible or nonlimiting on the voltammetric timescale), in accordance with the work by Compton and coworkers (80, 81, 96). The identity of the IL cation was found to have a minor

influence on k_s (59), in contrast to a later study, where it was shown that the IL anion can significantly influence the kinetics of the HER at Pt (60), in agreement with the discussions above (90).

A single PIL, $[N_{H,2,2,2}][NTf_2]$, was also investigated, and the HER mechanism (from $H[NTf_2]$) was found to be analogous to the AILs with respect to computational simulations. This is unsurprising, considering that the acidic constituent of the PIL, $H[NTf_2]$, is a superacid and therefore, complete proton transfer to the basic constituent, $[N_{2,2,2}]$, would be expected (23). As a result, the proton reduction is solely due to the $H[NTf_2]$ introduced into the neat $[N_{H,2,2,2}][NTf_2]$ (i.e., the H^+/H_2 process). The proton on the amine, $[N_{H,2,2,2}]^+$, can also be reduced. However, this species is a significantly weaker acid than $H[NTf_2]$, and therefore, much more negative potentials (approximately -0.9 V) must be reached before bulk proton reduction is observed (100).

The thermodynamics, kinetics, and mechanisms of the HER at a Pt electrode were also investigated in $[C_2mim][NTf_2]$ using range of nitrogen (R_xNH) acids (protonated amines or sulfonamides) as the proton source (60). Hydrogen evolution from weak nitrogen acids in the BH^+/H_2 process (the overall reaction shown in Equation 25) is a diffusion-controlled process that occurs in a potential region negative of the H^+/H_2 process, as shown in Figure 5a:



The $E^{0'}$ values of the investigated BH^+ acids span a potential window of approximately 0.9 V, representing a pK_a range of approximately 5.3 to 19.5 (derived as in Equation 10). Interestingly, the ΔE_p value, which is a qualitative indicator of electron-transfer kinetics, was found to increase with decreasing pK_a (compare 2-chloropyridinium and *N*-methylpyrrolidinium in Figure 5a) and increasing acid charge (compare diprotonated and monoprotated *o*-phenylenediaminium in Figure 5a). In addition, ΔE_p was found to differ significantly when comparing structurally disparate acids (protonated amines versus sulfonamides) of comparable strengths (compare pyridinium and saccharin in Figure 5a). Although the exact reason for these observations is not known, it was speculated that because Equation 22 is the rate determining step, the activation energy required to break the N–H bond is related to the heterolytic bond dissociation energy (i.e., pK_a) and structural factors (i.e., charge and chemical nature of the covalent bond).

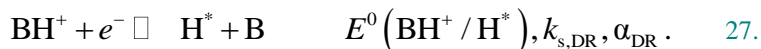
<COMP: PLEASE INSERT FIGURE 5 HERE>

Figure 5 (a) Cyclic voltammograms (normalized to unity with the reduction peak current, $I_{p,red}$) showing the hydrogen evolution reaction (HER), with the following proton sources (*top to bottom*): H[NTf₂], *o*-phenylenediaminium (diprotonated), 2,4-dichloropyridinium, 2-chloropyridinium, di(benzenesulfonyl)amide, anilinium, *o*-phenylenediaminium (monoprotonated), saccharin, pyridinium, *N*-methylimidazolium, and *N*-methylpyrrolidinium. The pK_a values calculated using Equation 10 are indicated in the figure. (b) Comparison of simulated (*red and blue lines*) and experimental (*black line*) cyclic voltammograms showing the HER, with 38.7 mM 2,4-dichloropyridinium as the proton source. The simulations were carried out using the CE mechanism only (Equations 22, 23, and 26; *red line*) or the CE + DR mechanism (Equations 22, 23, 26, and 27). Simulation parameters are as follows: $E^0(H^+/H^*) = -0.148$ V, $k_s = 0.022$ cm s⁻¹, $\alpha = 0.50$ (Equation 22, apparent values); $K_{dim} = 10^4$, $k_{dim} = 10^{16}$ M⁻¹ s⁻¹ (Equation 23); $E^0(BH^+/H^*) = -0.513$ V versus Fc/Fc⁺ ($pK_a = 6.2$), $k_{assoc} = 5 \times 10^8$ M⁻¹ s⁻¹ (Equation 26); $k_{s,DR} = 0.058$ cm s⁻¹, $\alpha_{DR} = 0.50$ (Equation 27, apparent values); $D_{H^+} = 3.1 \times 10^{-7}$ cm² s⁻¹, $D_{H_2} = 2.2 \times 10^{-5}$ cm² s⁻¹, $D_{BH^+} = 2.4 \times 10^{-7}$ cm² s⁻¹. $E^0(H^+/H_2) = -0.030$ V and $E^0(BH^+/H_2) = -0.395$ V, derived from $E^0(H^+/H^*)$, $E^0(BH^+/H^*)$ and K_{dim} . All experiments were carried out at a 1.6-mm-diameter Pt macrodisk electrode in [C₂mim][NTf₂] with a scan rate of 100 mV s⁻¹. Adapted with permission from Reference 60. Copyright 2015, American Chemical Society.

In order to simulate the BH⁺/H₂ process, two pathways were considered. The first is the CE pathway, whereby proton reduction via the mechanism described by Equations 22 and 23 is preceded by dissociation of BH⁺:



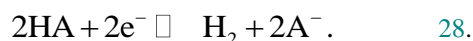
where k_{dissoc} and k_{assoc} are the dissociation and association rate constants, respectively. The second is a direct reduction (DR) pathway, where BH⁺ is discharged at the electrode surface without prior dissociation:



Again, it should be emphasized that k_s and α , are apparent values and therefore should not be assumed to have direct physical significance. In all simulations, k_{assoc} was set to 5×10^8 M⁻¹ s⁻¹, which should approximate the diffusion-controlled limit for a bimolecular reaction in [C₂mim][NTf₂] (78, 101). Simulations considering only the CE (Equations 22, 23, and 26) pathway or the CE + DR (Equations 22, 23, 26, and 27) pathways are shown in Figure 5b for the monoprotonated amine, 2,4-dichloropyridinium. Contrary to the mechanism proposed for benzoic acid (97–99), the CE pathway alone cannot support the mass transport–limited currents

observed experimentally due to the physical limitation of k_{dissoc} ($k_{\text{dissoc}} = K_{\text{a}}k_{\text{assoc}} \approx 300 \text{ s}^{-1}$), necessitating the inclusion of the parallel *DR* pathway in the simulations. Further simulations revealed that, under the experimental conditions, the *CE* pathway could only attain a diffusion-controlled current when $\text{p}K_{\text{a}} < 4$ [confirmed in a related study (61)]. The *DR* pathway becomes insignificant when $\text{p}K_{\text{a}} < 2$, which is in qualitative agreement with the studies by Evans and coworkers (54, 55) on the reduction of weak acids in dimethylsulfoxide.

In a related study (61), the thermodynamics, kinetics, and mechanisms of the HER at a Pt electrode were again investigated in the same IL, [C₂mim][NTf₂], but this time using a range of oxyacids (i.e., phenols, carboxylic acids, or sulfonic acids) as the proton source. Triflic acid, H[OTf], a well-known superacid in aqueous media, was shown to be a weak acid ($\text{p}K_{\text{a}} = 2.0$, derived using Equation 10) in [C₂mim][NTf₂] (conversely, H[NTf₂] was shown to behave as a strong acid in [C₂mim][OTf]), giving rise to a diffusion-controlled process that occurs in the potential region negative of the H⁺/H₂ process, as demonstrated in Figure 6:



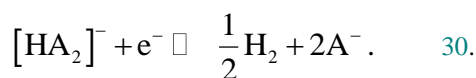
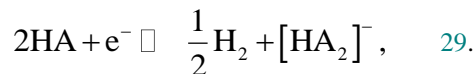
The HA/H₂ process, using H[OTf] as the proton source, was successfully simulated using the *CE* mechanism highlighted above (Equations 22, 23, and 26), in line with the theoretical predictions established in 60.

<COMP: PLEASE INSERT FIGURE 6 HERE>

Figure 6 Cyclic voltammograms ($\nu = 100 \text{ mV s}^{-1}$, normalized to unity with the reduction peak current, $I_{\text{p,red}}$) showing the hydrogen evolution reaction obtained at a 1.6-mm-diameter Pt macrodisk electrode in [C₂mim][NTf₂], with the following proton sources (*top to bottom*): H[NTf₂], H[OTf], naphthalene-2-sulfonic acid, H[OTs], methanesulfonic acid, trichloroacetic acid, dichloroacetic acid, malonic acid, *o*-hydroxybenzoic (salicylic) acid, pentachlorophenol, and glycolic acid. The $\text{p}K_{\text{a}}$ values calculated using Equation 10 are indicated in the figure. Abbreviation: Fc/Fc⁺, ferrocene/ferrocenium. Adapted with permission from Reference 61. Copyright 2015, American Chemical Society.

Proton reduction from a range of sulfonic or carboxylic acids ($5.9 \leq \text{p}K_{\text{a}} \leq 17.8$) occurs in two steps, as illustrated in Figures 6 and 7a. The electron stoichiometry of the two steps was confirmed to be 1:1 through semi-integration (69, 102). Based on this finding and what is known about oxyacids in aprotic media (103), including ILs (48), it was proposed that splitting of the proton reduction wave is caused by intermolecular hydrogen bonding between HA and its

conjugate base, A^- , forming the stable intermediate species, $[HA_2]^-$. This is a well-documented phenomenon (104, 105) known as homoassociation or homoconjugation, and in the present case, it occurs in the diffusion layer adjacent to the electrode surface in the potential region where the concentration of both species is comparable. Therefore, proton reduction from any (oxy)acid that undergoes homoassociation is expected to proceed via an *ECE* mechanism, where *C* is the homoassociation step, and the two processes observed voltammetrically are attributable to:



These equations account for the 1:1 electron stoichiometry observed experimentally.

<COMP: PLEASE INSERT FIGURE 7 HERE>

Figure 7 (a) Comparison of simulated (*circles*) and experimental (*lines*) cyclic voltammograms showing the HER obtained in $[C_2mim][NTf_2]$ from (*bottom to top*): 41.6 mM H[OTs], 41.6 mM H[OTs] + 44.0 mM $[C_2mim][OTs]$, and 41.2 mM H[OTs] + 86.1 mM $[C_2mim][OTs]$. Simulations were performed using the *DR* mechanism described by Equations 23, 27, and 31 using the following parameters: $K_{dim} = 10^4$, $k_{dim} = 10^{16} \text{ M}^{-1} \text{ s}^{-1}$ (Equation 23); $E^0(HA/H^*) = -0.512 \text{ V}$ versus Fc/Fc^+ ($pK_a = 6.2$), $k_{s,DR} = 0.09 \text{ cm/s}$, $\alpha_{DR} = 0.4$ (Equation 27, apparent values); $K_{homo} = 950$, $k_{homo} = 5 \times 10^8 \text{ M}^{-1} \text{ s}^{-1}$ (Equation 31); $D_{H_2} = 2.2 \times 10^{-5} \text{ cm}^2 \text{ s}^{-1}$; $D_{HA} = D_{A^-} = 2.6 \times 10^{-7} \text{ cm}^2 \text{ s}^{-1}$, $D_{[HA_2]^-} = 1.85 \times 10^{-7} \text{ cm}^2 \text{ s}^{-1}$. $E^0(HA/H_2) = -0.394 \text{ V}$, derived from $E^0(HA/H^*)$ and K_{dim} . (b) Cyclic voltammograms obtained from the HER, with H[OTs] as the proton source in (*bottom to top*): neat $[C_2mim][NTf_2]$, $[C_2mim][NTf_2]$ + 5.2 vol% PG and neat $[N_{H,2,2,2}][NTf_2]$. All experiments were carried out at a 1.6-mm-diameter Pt macrodisk electrode with a scan rate of 100 mV s^{-1} . Abbreviations: Fc/Fc^+ , ferrocene/ferrocenium; HER, hydrogen evolution reaction; PG, propylene glycol. Adapted with permission from Reference 61. Copyright 2015, American Chemical Society.

In order to simulate the $HA/[HA_2]^-/H_2$ processes, the previously established *DR* mechanism (Equations 23 and 27) was combined with the homoassociation equilibrium reaction:



Taking tosylic acid (H[OTs]) as the model acid species, and by assuming that k_{homo} occurs at the diffusion limited rate ($5 \times 10^8 \text{ M}^{-1} \text{ s}^{-1}$), the proton reduction response was simulated by assuming

a K_{homo} value of approximately 10^3 , as shown in **Figure 7a**. In addition, adding A^- (e.g., $[\text{OTs}]^-$) to a HA (e.g., $\text{H}[\text{OTs}]$) solution is expected to drive the equilibrium shown in **Equation 31** to the right, forming $[\text{HA}_2]^-$ at the expense of HA. This was observed experimentally and was predicted by the simulations, also shown in **Figure 7a**. Since the driving force for anionic homoassociation (i.e., K_{homo}) is intermolecular hydrogen bonding, this phenomenon is predicted to be suppressed through the addition of hydrogen-bonding solvents, promoting the formation of solvent–solute hydrogen bonds in preference to solute–solute. This was confirmed experimentally through the addition of ~5% (v/v) propylene glycol, as shown in **Figure 7b**. Alternatively, the hydrogen bond donating/accepting ability can be enhanced by varying the constituent cation/anion of the IL, demonstrated through the use of $[\text{N}_{\text{H},2,2,2}][\text{NTf}_2]$ ($[\text{N}_{\text{H},2,2,2}]^+$ is a relatively good hydrogen bond donor; see **Figure 7b**) or $[\text{C}_2\text{mim}][\text{N}(\text{CN})_2]$ ($[\text{N}(\text{CN})_2]^-$ is a relatively good hydrogen bond acceptor; not shown).

Despite the limitations in the simulations (simplified mechanisms using empirical rather than physically significant parameters), these studies (59–61) unveiled significant physical insights into the HER mechanism in IL media. Notably, although the characteristics of the H^+/H_2 process are relatively IL independent for a given anion (59), the thermodynamics, kinetics, and mechanisms of the BH^+/H_2 or HA/H_2 processes are strongly dependent upon the nature of the conjugate base (B or A^-) and the Lewis acid/base properties of the IL medium (60, 61).

4. CONCLUSIONS AND PROSPECTS

This review highlighted and discussed recent (electrochemical) studies on the energetics (thermodynamics) of proton transfer and electrode reaction mechanisms of the HER and HOR processes. The $\text{p}K_{\text{a}}$ scale has been the focus of many recent studies, with methods such as spectrophotometry, potentiometry, and voltammetry shown as robust methods for the quantification of (equilibrium) acidity in IL media. Although still in its infancy, especially when considering that each IL formulation will possess its own unique $\text{p}K_{\text{a}}$ scale (largely governed by the constituent anion), this work offers valuable insights into the influence of solvent (IL) properties (i.e., Lewis acidity/basicity, hydrogen bonding, polarity, etc.) on equilibrium acidity, expanded beyond conventional molecular solvent media. Furthermore, building on the so-called designer qualities of ILs, understanding the relationship between structure (i.e., anion and cation

properties) and function (i.e., proton availability or solvating ability) is an important step for tailoring these solvents for particular applications.

The H^+/H_2 process, although characterized extensively in aqueous media, has only been investigated in a limited range of ILs and almost exclusively on Pt electrodes over the past decade. The mechanism of this model inner-sphere process in ILs is proposed to be analogous to that in aqueous media, occurring via a combination of the well-established Volmer, Tafel and Heyrovsky reactions. The thermodynamics (i.e., E^0) of the H^+/H_2 process is IL dependent, as highlighted in the studies of $\text{p}K_{\text{a}}$ in this media, being predominantly governed by the identity of the constituent IL anion. However, the electrode kinetics of this process show a complex and generally poorly understood IL dependence and display considerably different voltammetric characteristics (e.g., voltammetric ΔE_{p} values) in even closely related IL formulations. ILs were identified early on for their potential as electrolytes in a range of electrochemical devices (e.g., PILs in fuel cells). Therefore, further work is necessary in this field to develop an understanding of how the characteristics of an IL formulation will influence the thermodynamics, kinetics, and mechanisms of inner-sphere reactions, such as the H^+/H_2 process. The ultimate goal, from an applications (i.e., fuel cell) perspective, would be to develop an IL formulation that facilitates facile HOR and ORR kinetics and fast anhydrous proton transport over a wide temperature range.

In conclusion, ILs are a diverse and versatile class of solvent that have garnered considerable attention over the past two decades as replacements for volatile molecular solvents in a range of applications. Nevertheless, as research in the field has matured over this time frame, the limits to our knowledge on fundamental processes (e.g., thermodynamics, kinetics, and mechanisms) in this type of medium have become apparent. Moving forward, developing an understanding of the factors that influence (electro)chemical reactivity in ILs, as exemplified in the studies summarized in this review, will undoubtedly facilitate the widespread adoption of these designer solvents in fields as diverse as energy technology to the biological sciences.

DISCLOSURE STATEMENT

The authors are not aware of any affiliations, memberships, funding, or financial holdings that might be perceived as affecting the objectivity of this review.

ACKNOWLEDGMENTS

C.L.B. acknowledges support from a Marie Curie Individual Fellowship (702048 NEIL). A.M.B. and J.Z. acknowledge support from the Australian Research Council.

<COMP: References have been added to/deleted from the Literature Cited section. Please renumber references in all manuscript elements (e.g., Literature Cited, text, figure captions, tables).>

LITERATURE CITED

1. Galinski M, Lewandowski A, Stepniak I. 2006. Ionic liquids as electrolytes. *Electrochim. Acta* 51:5567–80
2. Wilkes JS. 2002. A short history of ionic liquids—from molten salts to neoteric solvents. *Green Chem.* 4:73–80
3. Dean PM, Pringle JM, MacFarlane DR. 2010. Structural analysis of low melting organic salts: perspectives on ionic liquids. *Phys. Chem. Chem. Phys.* 12:9144–53
4. Dias AP, Papageorgiou N, Kalyanasundaram K, Grätzel M. 1996. Hydrophobic, highly conductive ambient-temperature molten salts. *Inorg. Chem.* 35:1168–78
5. Barrosse-Antle LE, Bond AM, Compton RG, O’Mahony AM, Rogers EI, Silvester DS. 2010. Voltammetry in room temperature ionic liquids: comparisons and contrasts with conventional electrochemical solvents. *Chemistry Asian J.* 5:202–30
6. Plechkova NV, Seddon KR. 2008. Applications of ionic liquids in the chemical industry. *Chem. Soc. Rev.* 37:123–50
7. Hapiot P, Lagrost C. 2008. Electrochemical reactivity in room-temperature ionic liquids. *Chem. Rev.* 108:2238–64
8. Welton T. 1999. Room-temperature ionic liquids. Solvents for synthesis and catalysis. *Chem. Rev.* 99:2071–83
9. Hallett JP, Welton T. 2011. Room-temperature ionic liquids: solvents for synthesis and catalysis. 2. *Chem. Rev.* 111:3508–76
10. Sun P, Armstrong DW. 2010. Ionic liquids in analytical chemistry. *Anal. Chim. Acta* 661:1–16

11. Zhang QH, Zhang SG, Deng YQ. 2011. Recent advances in ionic liquid catalysis. *Green Chem.* 13:2619–37
12. MacFarlane DR, Tachikawa N, Forsyth M, Pringle JM, Howlett PC, et al. 2014. Energy applications of ionic liquids. *Energy Environ. Sci.* 7:232–50
13. Fedorov MV, Kornyshev AA. 2014. Ionic liquids at electrified interfaces. *Chem. Rev.* 114:2978–3036
14. van Rantwijk F, Sheldon RA. 2007. Biocatalysis in ionic liquids. *Chem. Rev.* 107:2757–85
15. Wang H, Gurau G, Rogers RD. 2012. Ionic liquid processing of cellulose. *Chem. Soc. Rev.* 41:1519–37
16. Buzzeo MC, Evans RG, Compton RG. 2004. Non-haloaluminate room-temperature ionic liquids in electrochemistry—a review. *ChemPhysChem* 5:1106–20
17. Huddleston JG, Visser AE, Reichert WM, Willauer HD, Broker GA, Rogers RD. 2001. Characterization and comparison of hydrophilic and hydrophobic room temperature ionic liquids incorporating the imidazolium cation. *Green Chem.* 3:156–64
18. Schmeisser M, Illner P, Puchta R, Zahl A, van Eldik R. 2012. Gutmann donor and acceptor numbers for ionic liquids. *Chemistry Eur. J.* 18:10969–82
19. Yoshizawa M, Xu W, Angell CA. 2003. Ionic liquids by proton transfer: vapor pressure, conductivity, and the relevance of ΔpK_a from aqueous solutions. *J. Am. Chem. Soc.* 125:15411–19
20. Xu W, Angell CA. 2003. Solvent-free electrolytes with aqueous solution-like conductivities. *Science* 302:422–25
21. Farnicola A, Scrosati B, Ohno H. 2006. Potentialities of ionic liquids as new electrolyte media in advanced electrochemical devices. *Ionics* 12:95–102
22. Belieres J-P, Angell CA. 2007. Protic ionic liquids: preparation, characterization, and proton free energy level representation. *J. Phys. Chem. B* 111:4926–37
23. Greaves TL, Drummond CJ. 2008. Protic ionic liquids: properties and applications. *Chem. Rev.* 108:206–37
24. Bautista-Martinez JA, Tang L, Belieres J-P, Zeller R, Angell CA, Friesen C. 2009. Hydrogen redox in protic ionic liquids and a direct measurement of proton thermodynamics. *J. Phys. Chem. C* 113:12586–93

25. Angell CA, Ansari Y, Zhao ZF. 2012. Ionic liquids: past, present and future. *Faraday Discuss.* 154:9–27
26. Greaves TL, Drummond CJ. 2015. Protic ionic liquids: evolving structure-property relationships and expanding applications. *Chem. Rev.* 115:11379–448
27. Rana UA, Forsyth M, MacFarlane DR, Pringle JM. 2012. Toward protic ionic liquid and organic ionic plastic crystal electrolytes for fuel cells. *Electrochim. Acta* 84:213–22
28. Chen L, Guo S-X, Li F, Bentley C, Horne M, et al. 2016. Electrochemical reduction of CO₂ at metal electrodes in a distillable ionic liquid. *ChemSusChem* 9:1271–78
29. Seddon KR. 1997. Ionic liquids for clean technology. *J. Chem. Technol. Biotechnol.* 68:351–56
30. MacFarlane DR, Seddon KR. 2007. Ionic liquids—progress on the fundamental issues. *Austr. J. Chem.* 60:3–5
31. Armand M, Endres F, MacFarlane DR, Ohno H, Scrosati B. 2009. Ionic-liquid materials for the electrochemical challenges of the future. *Nat. Mater.* 8:621–29
32. Zhang J, Bond AM. 2005. Practical considerations associated with voltammetric studies in room temperature ionic liquids. *Analyst* 130:1132–47
33. Migliore A, Polizzi NF, Therien MJ, Beratan DN. 2014. Biochemistry and theory of proton-coupled electron transfer. *Chem. Rev.* 114:3381–465
34. Kreuer KD. 1996. Proton conductivity: materials and applications. *Chem. Mater.* 8:610–41
35. Mikkelsen M, Jørgensen M, Krebs FC. 2010. The teraton challenge. A review of fixation and transformation of carbon dioxide. *Energy Environ. Sci.* 3:43–81
36. Chen L, Li F, Bentley CL, Horne M, Bond AM, Zhang J. 2017. Electrochemical reduction of CO₂ with an oxide-derived lead nano-coralline electrode in dimcarb. *ChemElectroChem* 4:1402–10
37. Arico AS, Srinivasan S, Antonucci V. 2001. DMFCs: from fundamental aspects to technology development. *Fuel Cells* 1:133–61
38. Bard AJ, Fox MA. 1995. Artificial photosynthesis: solar splitting of water to hydrogen and oxygen. *Acc. Chem. Res.* 28:141–45
39. Lee SY, Ogawa A, Kanno M, Nakamoto H, Yasuda T, Watanabe M. 2010. Nonhumidified intermediate temperature fuel cells using protic ionic liquids. *J. Am. Chem. Soc.* 132:9764–73

40. Susan MABH, Noda A, Mitsushima S, Watanabe M. 2003. Brønsted acid-base ionic liquids and their use as new materials for anhydrous proton conductors. *Chem. Commun.* 8: 938–39
41. Nakamoto H, Watanabe M. 2007. Brønsted acid-base ionic liquids for fuel cell electrolytes. *Chem. Commun.* 24:2539–41
42. Diaz M, Ortiz A, Ortiz I. 2014. Progress in the use of ionic liquids as electrolyte membranes in fuel cells. *J. Membr. Sci.* 469:379–96
43. Silvester DS, Compton RG. 2006. Electrochemistry in room temperature ionic liquids: a review and some possible applications. *Z. Phys. Chem.* 220:1247–74
44. Perrin DD, Dempsey B, Serjeant EP. 1981. *pK_a Prediction for Organic Acids and Bases*. New York: Chapman & Hall
45. Barhdadi R, Troupel M, Comminges C, Laurent M, Doherty A. 2012. Electrochemical determination of pK_a of N-bases in ionic liquid media. *J. Phys. Chem. B* 116:277–82
46. Campbell ML, Waite BA. 1990. The K_a values of water and the hydronium ion for comparison with other acids. *J. Chem. Educ.* 67:386
47. Deng H, Li X, Chu Y, He J, Cheng J-P. 2012. Standard pK_a scales of carbon-centered indicator acids in ionic liquids: effect of media and structural implication. *J. Org. Chem.* 77:7291–98
48. Wang Z, Deng H, Li X, Ji PJ, Cheng JP. 2013. Standard and absolute pK_a scales of substituted benzoic acids in room temperature ionic liquids. *J. Org. Chem.* 78:12487–93
49. Bordwell FG. 1988. Equilibrium acidities in dimethyl sulfoxide solution. *Acc. Chem. Res.* 21:456–63
50. Barrette WC, Johnson HW, Sawyer DT. 1984. Voltammetric evaluation of the effective acidities (pK_a') for Brønsted acids in aprotic-solvents. *Anal. Chem.* 56:1890–98
51. Slater AM. 2014. The IUPAC aqueous and non-aqueous experimental pK_a data repositories of organic acids and bases. *J. Comput.-Aided Mol. Des.* 28:1031–34
52. Haynes W. 2014. *CRC Handbook of Chemistry and Physics: A Ready-Reference Book of Chemical and Physical Data*. Boca Raton, FL: CRC Press
53. Kütt A, Leito I, Kaljurand I, Sooväli L, Vlasov VM, et al. 2006. A comprehensive self-consistent spectrophotometric acidity scale of neutral Brønsted acids in acetonitrile. *J. Org. Chem.* 71:2829–38

54. Treimer SE, Evans DH. 1998. Electrochemical reduction of acids in dimethyl sulfoxide. CE mechanisms and beyond. *J. Electroanal. Chem.* 449:39–48
55. Treimer SE, Evans DH. 1998. Electrochemical reduction of acids in dimethyl sulfoxide. Comparison of weak C-H, N-H and O-H acids. *J. Electroanal. Chem.* 455:19–28
56. Serjeant EP, Dempsey B. 1979. *Ionisation Constants of Organic Acids in Aqueous Solution*. Oxford, UK: Pergamon
57. Qiang Z, Adams C. 2004. Potentiometric determination of acid dissociation constants (pK_a) for human and veterinary antibiotics. *Water Res.* 38:2874–90
58. Kütt A, Rodima T, Saame J, Raamat E, Mäemets V, et al. 2010. Equilibrium acidities of superacids. *J. Org. Chem.* 76:391–95
59. Bentley CL, Bond AM, Hollenkamp AF, Mahon PJ, Zhang J. 2014. Mass transport studies and hydrogen evolution at a platinum electrode using bis(trifluoromethanesulfonyl)imide as the proton source in ionic liquids and conventional solvents. *J. Phys. Chem. C* 118:22439–49
60. Bentley CL, Bond AM, Hollenkamp AF, Mahon PJ, Zhang J. 2015. Electrochemical proton reduction and equilibrium acidity (pK_a) in aprotic ionic liquids: protonated amines and sulfonamide acids. *J. Phys. Chem. C* 119:21828–39
61. Bentley CL, Bond AM, Hollenkamp AF, Mahon PJ, Zhang J. 2015. Electrochemical proton reduction and equilibrium acidity (pK_a) in aprotic ionic liquids: phenols, carboxylic acids, and sulfonic acids. *J. Phys. Chem. C* 119:21840–51
62. Mao C, Wang Z, Ji P, Cheng J-P. 2015. Is amine a stronger base in ionic liquid than in common molecular solvent? An accurate basicity scale of amines. *J. Org. Chem.* 80:8384–89
63. Wang Z, Li X, Ji P, Cheng JP. 2016. Absolute pK_a s of sulfonamides in ionic liquids: comparisons to molecular solvents. *J. Org. Chem.* 81:11195–200
64. Kanzaki R, Doi H, Song X, Hara S, Ishiguro S, Umebayashi Y. 2012. Acid-base property of *N*-methylimidazolium-based protic ionic liquids depending on anion. *J. Phys. Chem. B* 116:14146–52
65. Kanzaki R, Kodamatani H, Tomiyasu T, Watanabe H, Umebayashi Y. 2016. A pH scale for the protic ionic liquid ethylammonium nitrate. *Angew. Chem. Int. Ed.* 55:6266–69
66. Kanzaki R, Uchida K, Hara S, Umebayashi Y, Ishiguro S, Nomura S. 2007. Acid-base property of ethylammonium nitrate ionic liquid directly obtained using ion-selective field effect transistor electrode. *Chem. Lett.* 36:684–85

67. Bard AJ, Faulkner LR. 2001. *Electrochemical Methods: Fundamentals and Applications*. New York: Wiley
68. Compton RG, Banks CE. 2007. *Understanding Voltammetry*. London: World Sci.
69. Bentley CL, Bond AM, Hollenkamp AF, Mahon PJ, Zhang J. 2012. Advantages available in the application of the semi-integral electroanalysis technique for the determination of diffusion coefficients in the highly viscous ionic liquid 1-methyl-3-octylimidazolium hexafluorophosphate. *Anal. Chem.* 85:2239–45
70. Bentley CL, Bond AM, Hollenkamp AF, Mahon PJ, Zhang J. 2014. Applications of convolution voltammetry in electroanalytical chemistry. *Anal. Chem.* 86:2073–81
71. Bentley CL, Bond AM, Hollenkamp AF, Mahon PJ, Zhang J. 2015. Electroanalytical applications of semiintegral and convolution voltammetry in room-temperature ionic liquids. In *Electrochemistry in Ionic Liquids*, ed. AAJ Torriero, pp. 143–67. Berlin: Springer Int.
72. Rogers EI, Silvester DS, Poole DL, Aldous L, Hardacre C, Compton RG. 2008. Voltammetric characterization of the ferrocene|ferrocenium and cobaltocenium|cobaltocene redox couples in RTILs. *J. Phys. Chem. C* 112:2729–35
73. Gritzner G, Kuta J. 1984. Recommendations on reporting electrode-potentials in nonaqueous solvents. *Pure Appl. Chem.* 56:461–66
74. Stojanovic RS, Bond AM. 1993. Examination of conditions under which the reduction of the cobaltocenium cation can be used as a standard voltammetric reference process in organic and aqueous solvents. *Anal. Chem.* 65:56–64
75. Bentley CL, Li J, Bond AM, Zhang J. 2016. Mass-transport and heterogeneous electron-transfer kinetics associated with the ferrocene/ferrocenium process in ionic liquids. *J. Phys. Chem. C* 120:16516–25
76. Jaworski A, Donten M, Stojek Z, Osteryoung JG. 1999. Conditions of strict voltammetric reversibility of the H^+/H_2 couple at platinum electrodes. *Anal. Chem.* 71:243–46
77. Shuman MS. 1969. Nonunity electrode reaction orders and stationary electrode polarography. *Anal. Chem.* 41:142–46
78. Bentley CL, Bond AM, Hollenkamp AF, Mahon PJ, Zhang J. 2015. Voltammetric determination of the iodide/iodine formal potential and triiodide stability constant in conventional and ionic liquid media. *J. Phys. Chem. C* 119:22392–403

79. Barrette WC, Sawyer DT. 1984. Determination of dissolved hydrogen and effects of media and electrode materials on the electrochemical oxidation of molecular-hydrogen. *Anal. Chem.* 56:653–57
80. Meng Y, Aldous L, Belding SR, Compton RG. 2012. The hydrogen evolution reaction in a room temperature ionic liquid: mechanism and electrocatalyst trends. *Phys. Chem. Chem. Phys.* 14:5222–28
81. Meng Y, Aldous L, Belding SR, Compton RG. 2012. The formal potentials and electrode kinetics of the proton/hydrogen couple in various room temperature ionic liquids. *Chem. Commun.* 48:5572–74
82. Kibler LA. 2006. Hydrogen electrocatalysis. *ChemPhysChem* 7:985–91
83. Conway BE, Tilak BV. 2002. Interfacial processes involving electrocatalytic evolution and oxidation of H₂, and the role of chemisorbed H. *Electrochim. Acta* 47:3571–94
84. Greeley J, Jaramillo TF, Bonde J, Chorkendorff I, Norskov JK. 2006. Computational high-throughput screening of electrocatalytic materials for hydrogen evolution. *Nat. Mater.* 5:909–13
85. Trasatti S. 1972. Work function, electronegativity, and electrochemical behavior of metals. III. Electrolytic hydrogen evolution in acid solutions. *J. Electroanal. Chem.* 39:163–84
86. Rieger PH. 1994. *Electrochemistry*. New York: Chapman & Hall
87. Silvester DS, Aldous L, Hardacre C, Compton RG. 2007. An electrochemical study of the oxidation of hydrogen at platinum electrodes in several room temperature ionic liquids. *J. Phys. Chem. B* 111:5000–7
88. Silvester DS, Ward KR, Aldous L, Hardacre C, Compton RG. 2008. The electrochemical oxidation of hydrogen at activated platinum electrodes in room temperature ionic liquids as solvents. *J. Electroanal. Chem.* 618:53–60
89. Del Popolo MG, Kohanoff J, Lynden-Bell RM. 2006. Solvation structure and transport of acidic protons in ionic liquids: a first-principles simulation study. *J. Phys. Chem. B* 110:8798–803
90. Navarro-Suárez AM, Hidalgo-Acosta JC, Fadini L, Feliu JM, Suárez-Herrera MF. 2011. Electrochemical oxidation of hydrogen on basal plane platinum electrodes in imidazolium ionic liquids. *J. Phys. Chem. C* 115:11147–55

91. Tang YA, Lin L, Kumar A, Guo M, Sevilla M, Zeng XQ. 2017. Hydrogen electrooxidation in ionic liquids catalyzed by the NTf₂ radical. *J. Phys. Chem. C* 121:5161–67
92. Johnson L, Ejigu A, Licence P, Walsh DA. 2012. Hydrogen oxidation and oxygen reduction at platinum in protic ionic liquids. *J. Phys. Chem. C* 116:18048–56
93. Ejigu A, Walsh DA. 2014. The role of adsorbed ions during electrocatalysis in ionic liquids. *J. Phys. Chem. C* 118:7414–22
94. Goodwin SE, Walsh DA. 2016. Hydrogen electrooxidation under conditions of high mass transport in room-temperature ionic liquids and the role of underpotential-deposited hydrogen. *J. Phys. Chem. C* 120:11498–507
95. Aldous L, Silvester DS, Pitner WR, Compton RG, Lagunas MC, Hardacre C. 2007. Voltammetric studies of gold, protons, and HCl₂[−] in ionic liquids. *J. Phys. Chem. C* 111:8496–503
96. Meng Y, Aldous L, Compton RG. 2011. Electrochemistry of hydrogen in the room temperature ionic liquid 1-butyl-3-methylimidazolium bis(trifluoromethylsulfonyl)imide: dissolved hydrogen “lubricates” diffusional transport. *J. Phys. Chem. C* 115:14334–40
97. He W, Silvester DS, Streeter I, Aldous L, Hardacre C, Compton RG. 2009. Measuring the solubility of benzoic acid in room temperature ionic liquids using chronoamperometric techniques. *J. Phys. Org. Chem.* 22:69–76
98. Silvester DS, He W, Aldous L, Hardacre C, Compton RG. 2008. Electrochemical reduction of benzoic acid and substituted benzoic acids in some room temperature ionic liquids. *J. Phys. Chem. C* 112:12966–73
99. Meng Y, Norman S, Hardacre C, Compton RG. 2013. The electroreduction of benzoic acid: voltammetric observation of adsorbed hydrogen at a platinum microelectrode in room temperature ionic liquids. *Phys. Chem. Chem. Phys.* 15:2031–36
100. Goodwin SE, Smith DE, Gibson JS, Jones RG, Walsh DA. 2017. Electroanalysis of neutral precursors in protic ionic liquids and synthesis of high-ionicity ionic liquids. *Langmuir* 33:8436–46
101. Bentley CL, Bond AM, Hollenkamp AF, Mahon PJ, Zhang J. 2014. Electrode reaction and mass-transport mechanisms associated with the iodide/triiodide couple in the ionic liquid 1-ethyl-3-methylimidazolium bis(trifluoromethanesulfonyl)imide. *J. Phys. Chem. C* 118:29663–73

102. Grenness M, Oldham KB. 1972. Semiintegral electroanalysis: theory and verification. *Anal. Chem.* 44:1121–29
103. Bordwell FG, McCallum RJ, Olmstead WN. 1984. Acidities and hydrogen-bonding of phenols in dimethylsulfoxide. *J. Org. Chem.* 49:1424–27
104. Roses M. 1994. Ionic equilibria in nonaqueous solvents. 3. Effect of homoconjugation. *Anal. Chim. Acta* 285:391–99
105. Zielinska J, Makowski M, Maj K, Liwo A, Chmurzynski L. 1999. Acid-base and hydrogen-bonding equilibria in aliphatic amine and carboxylic acid systems in non-aqueous solutions. *Anal. Chim. Acta* 401:317–21